# Counter-rotating effects and entanglement dynamics in strongly coupled quantum-emitter–metallic-nanoparticle structures

Nikos Iliopoulos,[1] Ioannis Thanopulos,[2] Vassilios Yannopapas,[3] and Emmanuel Paspalakis[1]
[1]*Materials Science Department, School of Natural Sciences, University of Patras, Patras 265 04, Greece*
[2]*Department of Optics and Optometry, TEI of Western Greece, Aigio 251 00, Greece*
[3]*Department of Physics, National Technical University of Athens, Athens 157 80, Greece*

(Received 8 December 2017; revised manuscript received 30 January 2018; published 2 March 2018)

We study the spontaneous emission of a two-level quantum emitter next to a plasmonic nanoparticle beyond the Markovian approximation and the rotating-wave approximation (RWA) by combining quantum dynamics and classical electromagnetic calculations. For emitters with decay times in the picosecond to nanosecond time regime, as well as located at distances from the nanoparticle up to its radius, the dynamics with and without the RWA and the transition from the non-Markovian to the Markovian regime are investigated. For emitters with longer decay times, the Markov approximation proves to be adequate for distances larger than half the nanoparticle radius. However, the RWA is correct for all distances of the emitter from the nanoparticle. For short decay time emitters, the Markov approximation and RWA are both inadequate, with only the RWA becoming valid again at a distance larger than half the nanoparticle radius. We also show that the entanglement dynamics of two initially entangled qubits interacting independently with the nanoparticle may have a strong non-Markovian character when counter-rotating effects are included. Interesting effects such as entanglement sudden death, periodic entanglement revival, entanglement oscillations, and entanglement trapping are further observed when different initial two-qubit states and different distances between the qubit and the nanoparticle are considered.

DOI: 10.1103/PhysRevB.97.115402

## I. INTRODUCTION

When a quantum emitter is placed very close to the surface of a plasmonic nanostructure, the localized surface plasmons of the nanostructure dramatically influence the local photonic environment, promoting strong-coupling effects [1–4]. As a result, the population of the excited state of a two-level quantum emitter may exhibit strongly reversible, non-Markovian dynamics [5–16]. For example, population trapping effects of the excited state of the quantum emitter have been predicted [12,14] and attributed to the creation of a bound state in the electromagnetic continuum [14]. The non-Markovian response of the quantum emitter has been studied in the proximity of various plasmonic nanostructures, such as an infinite metallic surface [5], a flat metal-dielectric interface [6,14], a metallic nanosphere [7,10,12], a metallic nanorod [8], a metal nanoshell [9], and metallic and metal-dielectric nanocavities [11,15,16], as well as epsilon-and-mu-near-zero media [13]. Experimental results of strong coupling between a quantum emitter and a plasmonic nanostructure have recently been reported from several novel experiments [17–19]. The modified optical response of strongly coupled quantum emitters with plasmonic nanoparticles may have important applications in quantum technology [3,4,20] and may also have novel medical applications [21–23].

Additionally, a high degree of dissipation-driven entanglement between two quantum emitters (qubits) may occur via coupling of the qubits and the localized surface plasmons of plasmonic nanostructures [8,9,16,24–44]. The vast majority of the entanglement dynamics near plasmonic nanostructures has been analyzed in the weak-coupling regime, where the Markovian response of the system dynamics is applicable [24–44]. Recent studies have included strong-coupling effects and the non-Markovian response to the entanglement dynamics of two qubits coupled to a plasmonic nanostructure [8,9,16].

All of the above theoretical studies were performed under the assumption of the rotating-wave approximation (RWA) in the light-matter interaction. This is an excellent approximation in the weak-coupling regime, but in the strong and ultrastrong coupling regimes counter-rotating effects may appear and modify the quantum dynamics. In this work, we analyze the spontaneous emission dynamics of a quantum emitter near a spherical metallic nanoparticle (MNP) without making the RWA. To succeed we perform a unitary transformation in which the Hamiltonian that contains the counter-rotating terms is reduced to a Hamiltonian similar to that obtained with RWA [45–47]. By comparing the results of the population dynamics of the upper state of the two-level system with and without the RWA, we find that, under certain circumstances, for small distances of the emitter from the nanosphere, the inclusion of counter-rotating terms is crucial.

Moreover, we analyze the dynamics of two initially entangled qubits (modeled as two-level systems), where each one interacts locally, independent of each other, with a metallic nanosphere. We use the results without the RWA to study the dynamics of different initial states of the two-qubit system with a focus on the transition from the non-Markovian to the Markovian regime which occurs when varying the position of the quantum emitter with respect to the MNP. We find effects such as the sudden death of entanglement, entanglement revival, and entanglement trapping for quantum emitters positioned at different distances from the MNP. We note that both the Markovian and non-Markovian dynamics

 

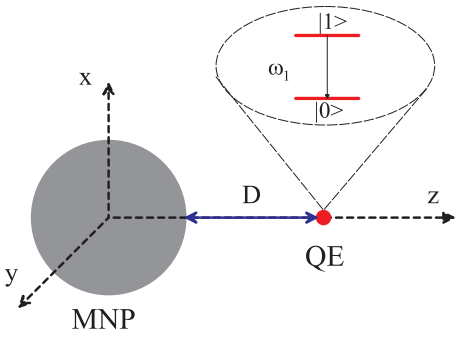


FIG. 1. The configuration of the two-level quantum emitter (QE) with resonance frequency $\omega_1$, placed at a distance $D$ from the surface of a spherical MNP.

of entanglement of two qubits interacting locally with either structureless or modified electromagnetic environments have been studied in several model photonic systems [48–56], such as the free-space vacuum [48,54], a cavity characterized by a Lorentzian coupling [50,53], and an isotropic photonic crystal [51], where analytical results are possible. Here, these effects are extended to a realistic plasmonic system, where we combine numerical electromagnetic calculations with quantum dynamics calculations without the RWA.

In the next section we present the theory for the spontaneous emission dynamics of a two-level quantum emitter next to a plasmonic nanostructure without applying the RWA. We perform a unitary transformation and write the equations of motion for the probability amplitudes for the system under study in terms of the electromagnetic Green's tensor. The differences of the derived equation and those under the application of the RWA are highlighted. Then, we present numerical results for the population dynamics of two specific quantum emitters near a spherical MNP for different positions of the emitter from the surface of the nanoparticle, with and without making the RWA. In Sec. III we present the dynamics of two initially entangled qubits, each one interacting locally, independent of each other, with a metallic nanosphere. We quantify entanglement using concurrence [57] and present the theory for the two-qubit system as well as use the results of Sec. II without the RWA to analyze the entanglement dynamics of the quantum emitters placed at different distances from the surface of the MNPs.

## II. DYNAMICS OF A QUANTUM EMITTER WITHOUT THE RWA

### A. Theory

We consider a two-level quantum emitter (QE) at distance $D$ from the surface of a spherical MNP, as shown in Fig. 1. The origin of the coordinate system coincides with the center of the sphere and the QE lies on the $z$ axis of the coordinate system.

The total Hamiltonian of the system is given by

$$\hat{H} = \hat{H}_A + \hat{H}_F + \hat{H}_{AF}, \tag{1}$$

where the first term gives the energy of the quantum emitter, the second term gives the energy of the electromagnetic field, and the third term gives the interaction between the emitter and the electromagnetic field. Here, we use the multipolar coupling scheme under the Power-Zienau-Woolley transformation [58] and do not use the minimal-coupling scheme as, for example, in Refs. [59,60]. As a result, we can write $\hat{H}_{AF} = -\boldsymbol{\mu}\cdot\mathbf{E}(\mathbf{r})$, with $\boldsymbol{\mu}$ being the electric dipole moment of the quantum emitter and

$$\hat{\mathbf{E}}(\mathbf{r}) = \hat{\mathbf{E}}^{(+)}(\mathbf{r}) + \hat{\mathbf{E}}^{(-)}(\mathbf{r}), \qquad \hat{\mathbf{E}}^{(-)}(\mathbf{r}) = [\hat{\mathbf{E}}^{(+)}(\mathbf{r})]^\dagger, \tag{2}$$

$$\hat{\mathbf{E}}^{(+)}(\mathbf{r}) = \int_0^\infty d\omega \underline{\hat{\mathbf{E}}}(\mathbf{r},\omega), \tag{3}$$

$$\underline{\hat{\mathbf{E}}}(\mathbf{r},\omega) = i\sqrt{\frac{\hbar}{\pi\epsilon_0}}\frac{\omega^2}{c^2}\int d^3\mathbf{r}'\sqrt{\epsilon_I(\mathbf{r}',\omega)}\mathbf{G}(\mathbf{r},\mathbf{r}',\omega)\cdot\hat{\mathbf{f}}(\mathbf{r}',\omega), \tag{4}$$

where $\hat{\mathbf{f}}^\dagger(\mathbf{r}',\omega)$ and $\hat{\mathbf{f}}(\mathbf{r}',\omega)$ are the creation and annihilation operators of the electromagnetic field obeying the usual commutation relations [59]. $\mathbf{G}(\mathbf{r},\mathbf{r}',\omega)$ is the classical electromagnetic Green's tensor, which obeys the equation

$$\left[\frac{\omega^2}{c^2}\epsilon(\mathbf{r},\omega) - \nabla\times\nabla\times\right]\mathbf{G}(\mathbf{r},\mathbf{r}',\omega) = -\mathbb{I}\delta(\mathbf{r}-\mathbf{r}'), \tag{5}$$

where $\epsilon(\mathbf{r},\omega)$ is the space- and frequency-dependent dielectric function of our system [$\epsilon_I(\mathbf{r},\omega)$ is just the imaginary part of it]. Also, $\mathbb{I}$ is the dyadic unit tensor.

Using the above equations we write the total Hamiltonian of our system, without using the RWA, as

$$\begin{aligned}\hat{H} =\ & \hbar\omega_1|1\rangle\langle 1| + \int d^3\mathbf{r}'\int_0^\infty d\omega\hbar\omega\hat{\mathbf{f}}^\dagger(\mathbf{r}',\omega)\cdot\hat{\mathbf{f}}(\mathbf{r}',\omega)\\ &+\hbar\int_{-\infty}^\infty d\omega\int d^3\mathbf{r}' g(\mathbf{r}',\omega)(|0\rangle\langle 1| + |1\rangle\langle 0|)\\ &\times[\hat{\mathbf{f}}^\dagger(\mathbf{r}',\omega) + \hat{\mathbf{f}}(\mathbf{r}',\omega)],\end{aligned} \tag{6}$$

where $\hat{H}_A$, $\hat{H}_F$, and $\hat{H}_{AF}$ are, respectively, the first (assuming that the energy of state $|0\rangle$ is zero), second, and third terms. Additionally, we have set

$$g(\mathbf{r}',\omega) = -i\sqrt{\frac{\hbar}{\pi\epsilon_0}}\frac{\omega^2}{c^2}\sqrt{\epsilon_I(\mathbf{r}',\omega)}\mathbf{G}(\mathbf{r},\mathbf{r}',\omega)\cdot\frac{\boldsymbol{\mu}}{\hbar}, \tag{7}$$

which is the quantum-emitter–field coupling constant.

We make the unitary transformation $\hat{U} = e^{iS}$ [45–47], with

$$\begin{aligned}S =\ & -i\int d^3\mathbf{r}'\int_{-\infty}^\infty d\omega\frac{g(\mathbf{r}',\omega)}{\omega_1+\omega}[\mathbf{f}^\dagger(\mathbf{r}',\omega) - \mathbf{f}(\mathbf{r}',\omega)]\\ &\times(|0\rangle\langle 1| + |1\rangle\langle 0|)\,.\end{aligned} \tag{8}$$

With this transformation the new Hamiltonian $\hat{H}'$ resembles the form of the Hamiltonian obtained if we had used the RWA. Then, after some algebra and removing the self-energy of the electron, $-\hbar\int d^3\mathbf{r}'\int_{-\infty}^\infty d\omega\frac{g^2(\mathbf{r}',\omega)}{\omega}(|0\rangle\langle 0| + |1\rangle\langle 1|)$, we obtain

$$\begin{aligned}\hat{H}' =\ & \hbar\left(\omega_1 + \Delta\omega_{ndy}^{(1)}\right)|1\rangle\langle 1| + \hbar\Delta\omega_{ndy}^{(0)}|0\rangle\langle 0|\\ &+\int d^3\mathbf{r}'\int_0^\infty d\omega\hbar\omega\hat{\mathbf{f}}^\dagger(\mathbf{r}',\omega)\cdot\hat{\mathbf{f}}(\mathbf{r}',\omega)\\ &+\hbar\int d^3\mathbf{r}'\int_{-\infty}^\infty d\omega V(\mathbf{r}',\omega)\\ &\times[\hat{\mathbf{f}}^\dagger(\mathbf{r}',\omega)|0\rangle\langle 1| + \hat{\mathbf{f}}(\mathbf{r}',\omega)|1\rangle\langle 0|],\end{aligned} \tag{9}$$

where we have set

$$V(\mathbf{r}',\omega)=\frac{2\omega_1 g(\mathbf{r}',\omega)}{\omega_1+\omega}, \tag{10}$$

which plays the same role as $g(\mathbf{r}',\omega)$ in the nontransformed Hamiltonian of Eq. (6), and

$$\Delta\omega_{ndy}^{(0)}=\int d^3\mathbf{r}'\int_{-\infty}^{\infty}d\omega\frac{g^2(\mathbf{r}',\omega)}{\omega}\frac{\omega_1(\omega_1+\omega)}{(\omega_1+\omega)^2}, \tag{11}$$

$$\Delta\omega_{ndy}^{(1)}=\int d^3\mathbf{r}'\int_{-\infty}^{\infty}d\omega\frac{g^2(\mathbf{r}',\omega)}{\omega}\frac{\omega_1(\omega_1-\omega)}{(\omega_1+\omega)^2} \tag{12}$$

are the nondynamical energy shifts. Also, in the above calculations we ignored the terms (wherever they appeared) $\mathbf{f}^\dagger(\mathbf{r}',\omega)\cdot\mathbf{f}^\dagger(\mathbf{r}',\omega)$ and $\mathbf{f}(\mathbf{r}',\omega)\cdot\mathbf{f}(\mathbf{r}',\omega)$; terms of the form $\mathbf{f}^\dagger(\mathbf{r}',\omega)\cdot\mathbf{f}(\mathbf{r}',\omega)$ are also ignored since $\mathbf{f}^\dagger(\mathbf{r}',\omega)\cdot\mathbf{f}(\mathbf{r}',\omega)|\{0\}\rangle=0$, with $|\{0\}\rangle$ being the vacuum state of the electromagnetic field.

Now we take a general state of our composite system (quantum emitter plus electromagnetic field). Such a general state has the form

$$|\psi(t)\rangle=c_1(t)e^{-i\left(\omega_1+\Delta\omega_{ndy}^{(1)}\right)t}|1,\{0\}\rangle+\int d^3\mathbf{r}'\times\int_{-\infty}^{\infty}d\omega c_0(\mathbf{r}',\omega,t)e^{-i\left(\omega+\Delta\omega_{ndy}^{(0)}\right)t}|0,\{\mathbf{1}_{\mathbf{r}',\omega}\}\rangle, \tag{13}$$

with $|\{\mathbf{1}_{\mathbf{r}',\omega}\}\rangle=\mathbf{f}^\dagger(\mathbf{r}',\omega)|\{0\}\rangle$. We substitute this general state and the transformed Hamiltonian of Eq. (9) into the time-dependent Schrödinger equation; we find the differential equations for the probability amplitudes as

$$\dot{c}_1(t)=-i\int d^3\mathbf{r}'\int_{-\infty}^{\infty}d\omega V(\mathbf{r}',\omega)e^{-i(\omega-\omega_1')t}c_0(\mathbf{r}',\omega,t), \tag{14}$$

$$\dot{c}_0(\mathbf{r}',\omega,t)=-iV(\mathbf{r}',\omega)e^{i(\omega-\omega_1')t}c_1(t), \tag{15}$$

with $\omega_1'=\omega_1+\Delta\omega_{ndy}^{(1)}-\Delta\omega_{ndy}^{(0)}$.

Integrating Eq. (15) formally and replacing $c_0(\mathbf{r}',\omega,t)$ in Eq. (14), we obtain the integro-differential equation for the probability amplitude $c_1(t)$ as

$$\dot{c}_1(t)=i\int_0^t dt'K(t-t')c_1(t'), \tag{16}$$

where the Kernel function is given by

$$K(\tau)=ie^{i\omega_1'\tau}\int d^3\mathbf{r}'\int_{-\infty}^{\infty}d\omega V^2(\mathbf{r}',\omega)e^{-i\omega\tau}, \tag{17}$$

with $\tau=t-t'$.

Using the Green's tensor properties, we can rewrite the Kernel function as

$$K(\tau)=ie^{i\omega_1'\tau}\int_0^{\infty}d\omega J(\omega)e^{-i\omega\tau}, \tag{18}$$

with the spectral density

$$J(\omega)=\left(\frac{2\omega_1}{\omega_1+\omega}\right)^2\int d^3\mathbf{r}'\frac{\omega^4}{\hbar\pi\epsilon_0c^4}\epsilon_I(\mathbf{r}',\omega)\boldsymbol{\mu}\cdot\times\mathbf{G}(\mathbf{r},\mathbf{r}',\omega)\mathbf{G}^\star(\mathbf{r},\mathbf{r}',\omega)\cdot\boldsymbol{\mu}\,. \tag{19}$$

Assuming that we have linear polarization and the magnitude of the electric dipole moment is $\mu$, then we can rewrite the spectral density as

$$\begin{aligned}J(\omega)&=\left(\frac{2\omega_1}{\omega_1+\omega}\right)^2\frac{\omega^2\mu^2}{\hbar\pi\epsilon_0c^2}\int d^3\mathbf{r}'\epsilon_I(\mathbf{r}',\omega)\frac{\omega^2}{c^2}\\&\quad\times\mathbf{G}_k(\mathbf{r},\mathbf{r}',\omega)\mathbf{G}_k^\star(\mathbf{r},\mathbf{r}',\omega)\\&=\left(\frac{2\omega_1}{\omega_1+\omega}\right)^2\frac{\omega^2\mu^2}{\hbar\pi\epsilon_0c^2}\mathrm{Im}[\mathbf{G}_k(\mathbf{r},\mathbf{r},\omega)],\end{aligned} \tag{20}$$

using again the Green's function properties. Here, $k$ determines the direction of the electric dipole. Moreover, the decay rate of the atom $\Gamma_k(\omega)$ in the presence of the MNP is expressed by the relation [12]

$$\Gamma_k(\omega)=\frac{2\mu^2\omega^2}{\epsilon_0\hbar c^2}\mathrm{Im}[\mathbf{G}_k(\mathbf{r},\mathbf{r},\omega)]. \tag{21}$$

As a result, the spectral density takes the form

$$\begin{aligned}J(\omega)&=\left(\frac{2\omega_1}{\omega_1+\omega}\right)^2\frac{1}{2\pi}\Gamma_k(\omega)\\&=\left(\frac{2\omega_1}{\omega_1+\omega}\right)^2\frac{1}{2\pi}\lambda_k(\omega,D)\Gamma_0(\omega)\\&=\left(\frac{2\omega_1}{\omega_1+\omega}\right)^2\frac{\Gamma_0(\omega_1)}{2\pi}\lambda_k(\omega,D)\left(\frac{\omega}{\omega_1}\right)^3,\end{aligned} \tag{22}$$

where $\Gamma_0(\omega)$ is the spontaneous emission rate in free space given by

$$\Gamma_0(\omega)=\frac{\omega_1^3\mu^2}{3\pi\hbar\epsilon_0c^3}\left(\frac{\omega}{\omega_1}\right)^3\equiv\Gamma_0(\omega_1)\left(\frac{\omega}{\omega_1}\right)^3 \tag{23}$$

and $\lambda_k(\omega,D)$ is the directional enhancement factor of the spontaneous emission rate in free space due to the placement of the quantum emitter at distance $D$ from a MNP [12].

Also,

$$\omega_1'=\omega_1-\left(\Delta\omega_{ndy}^{(0)}-\Delta\omega_{ndy}^{(1)}\right)\equiv\omega_1-\frac{\Delta E_{ndy}}{\hbar}, \tag{24}$$

with

$$\Delta E_{ndy}=\hbar\int_0^{\infty}d\omega\frac{2\omega_1}{(\omega_1+\omega)^2}\frac{\Gamma_0(\omega_1)}{2\pi}\lambda_k(\omega,D)\left(\frac{\omega}{\omega_1}\right)^3. \tag{25}$$

We note that when using the RWA, the nondynamical energy shift $\Delta E_{ndy}$ is zero, and as a result the characteristic frequency of the atom $\omega_1$ remains the same. We also note that the spectral density $J(\omega)$ has the extra term $(\frac{2\omega_1}{\omega+\omega_1})^2$ when we do not use the RWA.

### B. Numerical results for a single quantum emitter

Here, we consider a 5-nm silver sphere. Its electromagnetic response is described by a Drude dielectric function, $\epsilon_m(\omega)=\epsilon_{m,\infty}-\omega_p^2/(\omega^2+i\omega\gamma)$, characterized by its plasma frequency $\omega_p=9.176$ eV, high-frequency component $\epsilon_{m,\infty}=3.718$ eV, and Ohmic losses $\gamma=0.021$ eV [12,61]. The enhancement factor for the free-space decay rate of the QE due to the presence of such a MNP as a function of frequency $\omega$ at distance $D$ has been calculated using an electromagnetic Green's tensor

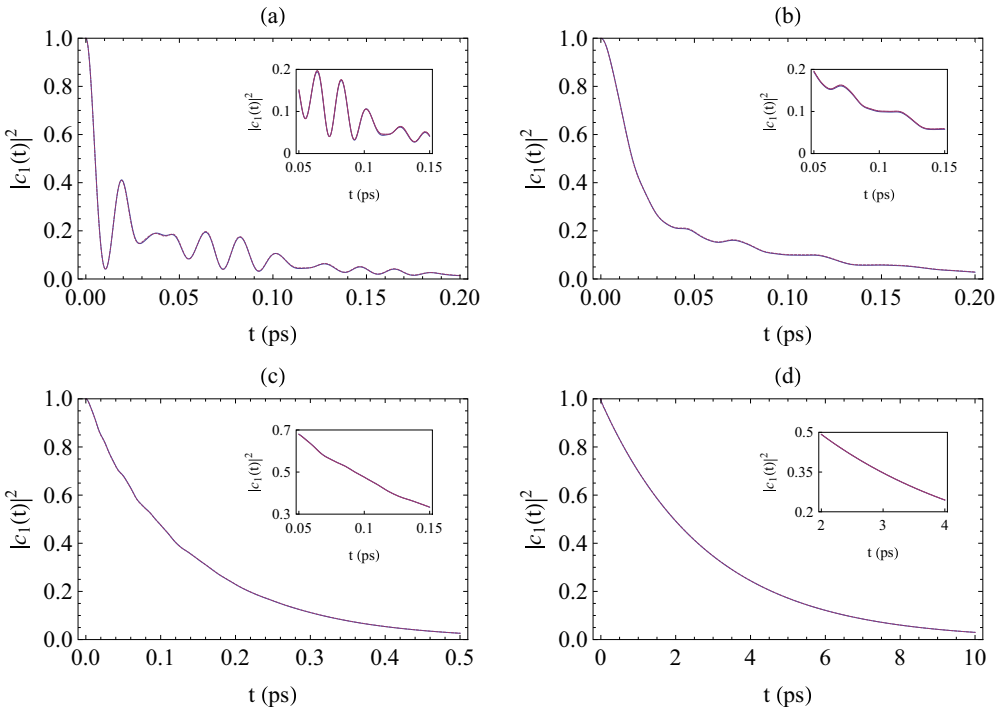


FIG. 2. Plot of the population evolution of state $|1\rangle$ with (blue solid line) and without (red dashed line) applying the RWA for a QD with $\hbar\omega_1 = 4.16$ eV at distance (a) $D = 1$ nm, (b) $D = 2$ nm, (c) $D = 3$ nm, and (d) $D = 5$ from the MNP. The inset in each panel shows a certain part of the evolution where the differences between the RWA and non-RWA cases are more visible. We note that the two curves are practically indistinguishable in all panels.

technique [62]; the results for the enhancement factor are given in Fig. 2 of Ref. [12].

In this work, we use state-of-the-art quantum emitters with transition frequencies in the optical regime, like quantum dots (QDs) and $J$ aggregates (J-AGRs), with the corresponding decay times $\tau_0 = 1/\Gamma_0(\omega_1) \approx 4$ ns [63] and 70 ps [64]. In the figures below, we study the population dynamics $|c_1(t)|^2$ of a QD or a J-AGR for different distances from the MNP and for the initial state $|1\rangle$, with and without applying the RWA. In all figures we assume that the quantum-emitter electric dipole is in the radial direction. The calculations are performed by numerical solution of Eq. (16) using the effective mode differential equation method [12,65].

Figure 2 shows how the population of the upper state $|1\rangle$ evolves with time for a QD. In Fig. 2(a), the QD is located at distance $D = 1$ nm from the MNP. Strong non-Markovian dynamics featuring population oscillations is observed. The non-Markovian characteristics of the dynamics become weaker as the distance between the quantum emitter and the MNP increases; they essentially disappear at $D = 5$ nm, where the dynamics is obviously Markovian. Moreover, the counter-rotating terms affect the population evolution, when compared with the population evolution within the RWA, as shown in all the figures. This can be explained by the fact that the nondynamical energy shift $\Delta E_{ndy}$ is really small at all distances. More specifically, for $D = 1$ nm, $\Delta E_{ndy} = 0.0014$ eV; for $D = 2$ nm, $\Delta E_{ndy} = 0.0002$ eV; for $D = 3$ nm, $\Delta E_{ndy} = 0.00006$ eV; and for $D = 5$ nm, $\Delta E_{ndy} = 0.00001$ eV.

In Fig. 3 we show the dynamics of a J-AGR which has the same energy as the QD. Due to its shorter $\tau_0$, the interaction of the J-AGR with the MNP and, as a result, the population dynamics will display many more oscillations in comparison to the QD case [12]. In Fig. 3(a) we see that the population $|c_1(t)|^2$ has really intense oscillations with very large amplitude for both the RWA and no-RWA cases. Strong non-Markovian effects are also present at larger distances, as shown in Figs. 3(b) and 3(c). The oscillations in the case of a J-AGR are also preserved even at $D = 5$ nm [Fig. 3(d)] from the MNP, whereas for a QD the dynamics is Markovian. We also observe that the differences between the RWA and no-RWA cases are notable, especially at small distances $D$. This is due to the fact that the nondynamical energy shift $\Delta E_{ndy}$ takes larger values at smaller distances. Specifically, at $D = 1$ nm we have $\Delta E_{ndy} = 0.0818$ eV, while for $D = 5$ nm it is only $\Delta E_{ndy} = 0.0006$ eV. In order to identify the origin of this transition more clearly, we have calculated the corresponding values of $\Delta E_{ndy}$ for the distances $D = 2$ nm and $D = 3$ nm, which are 0.0134 and 0.0037 eV, respectively.

Another interesting issue here is the fact that the oscillations of the population are preserved for much longer times (see Fig. 4). More specifically, as shown in Figs. 4(a) and 4(b), the population evolution has an oscillatory character, indicating that there is a permanent population exchange between the quantum emitter and the modified electromagnetic continuum, leading to the effect of oscillatory population trapping [12]. Such oscillations are present with or without implementing the RWA. The main modification which takes place when taking into account the counter-rotating terms is a phase difference which becomes more important at later times. Otherwise, the period and amplitude of the oscillation remain

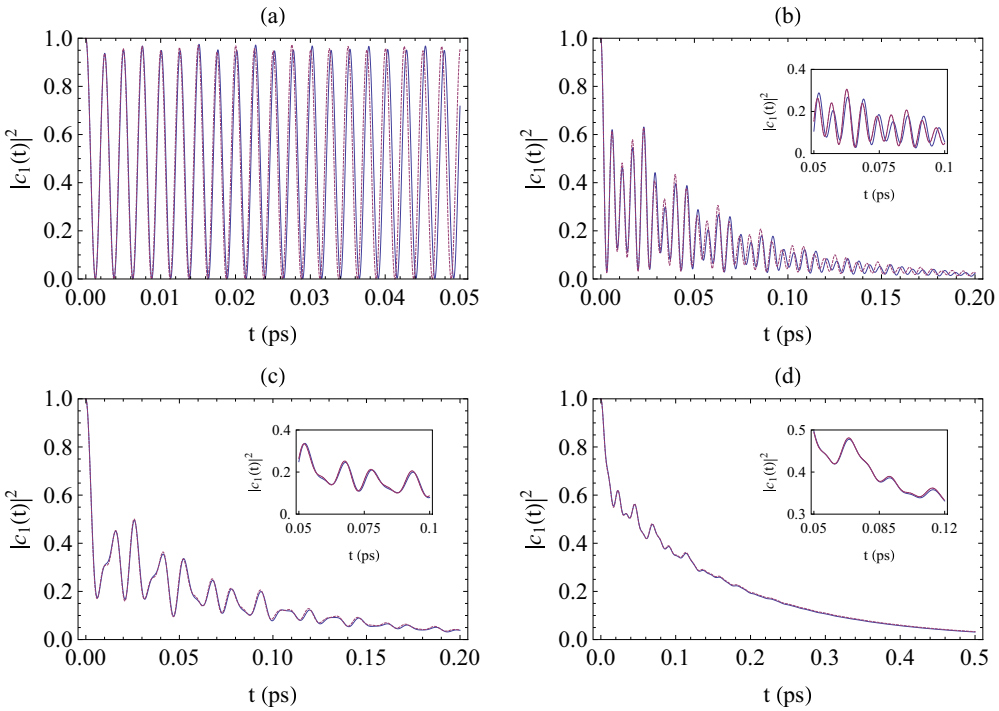


FIG. 3. The same as in Fig. 2, but for a J-AGR with $\hbar\omega_1 = 4.16$ eV.

almost unaffected by the counter-rotating terms. However, at distance $D = 1.85$ nm, the phenomenon of steady-state population trapping is observed [12,14]. The interaction of the two-level system with its environment is not as strong as for $D = 1$ nm and $D = 1.5$ nm, where the oscillatory character of the population evolution is dominant; at the same time, the interaction is not as weak as at $D = 2$ nm, in which case the excited-level population vanishes in the long-time limit. Essentially, at $D = 1.85$ nm, we observe an intermediate case where the population of the excited level is "trapped" in a steady state. We note that although the time evolution of $|c_1(t)|^2$ is approximately the same at early stages whether we apply the RWA or not, the trapping is affected only when we take into account the counter-rotating terms since $|c_1(t)|^2$ takes smaller values compared to the values it assumes when RWA is employed [the inset in Fig. 4(c) highlights this difference].

## III. ENTANGLEMENT DYNAMICS

### A. Theory

In the preceding section we described the dynamics of a single two-level system interacting with the modified electromagnetic field modes near a MNP, with and without applying the RWA, where we demonstrated how the counter-rotating terms may affect the time evolution of the population. Now, we consider the case of two identical two-level quantum emitters, $A$ and $B$, forming two qubits. We position each qubit near a MNP, and we place the two systems far apart, such that they do not interact with each other. Since the two qubits interact with different, noninteracting environments, we can factorize the total time evolution into two parts. Thus, if we assume that for each qubit we have $\rho^A_{ii'}(t) = \sum_{nn'} A^{nn'}_{ii'}(t)\rho^A_{nn'}(0)$ and $\rho^B_{jj'}(t) = \sum_{mm'} B^{mm'}_{jj'}(t)\rho^B_{mm'}(0)$, then for the two-qubit system we take [50,51,56]

$$\rho_{ii',jj'}(t) = \sum_{nn',mm'} A^{nn'}_{ii'}(t)B^{mm'}_{jj'}(t)\rho_{nn',mm'}(0), \tag{26}$$

with $i,j,n,m = 0,1$. Assuming now that the environment has zero temperature and the qubit at $t = 0$ is in a general superposition state, the reduced density matrix $\rho^{(1)}(t)$ for the single qubit is [50,51,56]

$$\rho^{(1)}(t) = \begin{bmatrix} \rho^{(1)}_{11}(0)|c_1(t)|^2 & \rho^{(1)}_{10}(0)c_1(t) \\ \rho^{(1)}_{01}(0)c_1{}^*(t) & \rho^{(1)}_{00}(0) + \rho^{(1)}_{11}(0)(1 - |c_1(t)|^2) \end{bmatrix}. \tag{27}$$

Equation (27) shows that, besides initial conditions, the single-qubit dynamics depends only on $c_1(t)$ obtained with Eq. (16). This function essentially contains information about the interaction of the qubit with its environment and, more specifically, how this interaction evolves with time.

Next, we calculate the density matrix of the composite two-qubit system. Since the qubits are identical, the density matrix of our composite system is calculated by the tensor product $\rho^{(2)}(t) = \rho^{(1)}_A(t) \otimes \rho^{(1)}_B(t)$. Additionally, we need a new basis for the composite system which is given by $\mathcal{B} = \{|\mathcal{K}\rangle \equiv |11\rangle, |\mathcal{L}\rangle \equiv |10\rangle, |\mathcal{M}\rangle \equiv |01\rangle, |\mathcal{N}\rangle \equiv |00\rangle\}$. The analytical expressions for the elements of the density matrix of the composite system $\rho^{(2)}(t)$ can be found elsewhere [51]. As for the case of the single-qubit dynamics, the elements of $\rho^{(2)}(t)$ depend only on the function $c_1(t)$.

We then proceed to the description of the measure of entanglement used in our work. We will use concurrence as a measure of entanglement [57]. The computation of concurrence is based on the density matrix of the composite system.

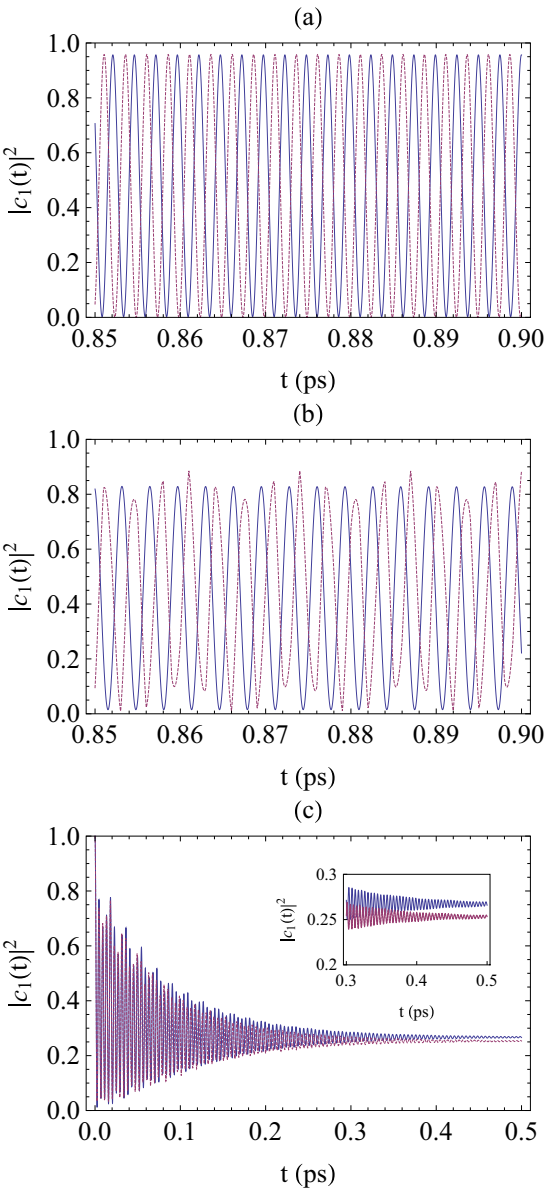


FIG. 4. Population dynamics of the upper state $|1\rangle$ of a J-AGR with $\hbar\omega_1 = 4.16$ eV with the RWA (blue solid line) and without the RWA (red dashed line) at distances (a) $D = 1$ nm, (b) $D = 1.5$ nm, and (c) $D = 1.85$ nm from the MNP. The inset in Fig. 4(c) highlights the phenomenon of population trapping.

Thus, we have to compute first the matrix $R = \rho^{(2)}(t)(\sigma_y^A \otimes \sigma_y^B)\rho^{(2)*}(t)(\sigma_y^A \otimes \sigma_y^B)$, where $\sigma_y^i$, with $i = A, B$, are the Pauli matrices of the two two-level systems, respectively. Then, we diagonalize the matrix $R$, compute its eigenvalues $\lambda_n$, with $n = 1,2,3,4$, and, finally, calculate the concurrence provided by $C \equiv \max[0, \sqrt{\lambda_1} - \sqrt{\lambda_2} - \sqrt{\lambda_3} - \sqrt{\lambda_4}]$, where $\lambda_1 > \lambda_2 > \lambda_3 > \lambda_4$. Concurrence takes values from 0 (no entanglement for the system) to 1 (maximum entanglement).

We assume that our composite system is prepared in the Bell-like states

$$|\Phi\rangle = a|01\rangle + e^{i\chi}\sqrt{1-a^2}|10\rangle, \tag{28}$$

$$|\Psi\rangle = a|00\rangle + e^{i\chi}\sqrt{1-a^2}|11\rangle, \tag{29}$$

with $0 \leqslant a \leqslant 1$. For simplicity, in this study, we consider $\chi = 0$. Following Ref. [56], Bell-like states are a certain kind of $X$ state which are commonly used in quantum information and quantum computation. For $a = 0$ or 1, Eqs. (28) and (29) become separate states, while for $a = 1/\sqrt{2}$ they become maximally entangled states (Bell states). As a result, using a Bell-like state as the initial state of our system allows us to control the degree of entanglement by changing the parameter $a$. The density matrix of the composite system for the initial states of Eqs. (28) and (29) is given after some algebra by

$$\rho^{(2)}(t) = \begin{bmatrix} \rho^{(2)}_{\mathcal{KK}} & 0 & 0 & \rho^{(2)}_{\mathcal{NK}} \\ 0 & \rho^{(2)}_{\mathcal{LL}} & \rho^{(2)}_{\mathcal{LM}} & 0 \\ 0 & \rho^{(2)}_{\mathcal{ML}} & \rho^{(2)}_{\mathcal{MM}} & 0 \\ \rho^{(2)}_{\mathcal{KN}} & 0 & 0 & \rho^{(2)}_{\mathcal{NN}} \end{bmatrix}. \tag{30}$$

Based on the above formalism, concurrence is calculated by

$$C = \max\{0, C_1, C_2\}, \tag{31}$$

where $C_1 = 2(|\rho^{(2)}_{\mathcal{KN}}| - \sqrt{\rho^{(2)}_{\mathcal{LL}}\rho^{(2)}_{\mathcal{MM}}})$ and $C_2 = 2(|\rho^{(2)}_{\mathcal{LM}}| - \sqrt{\rho^{(2)}_{\mathcal{KK}}\rho^{(2)}_{\mathcal{NN}}})$ since each eigenvalue of $\rho^{(2)}(t)$ given by Eq. (30) is twofold degenerate. If our initial state is $|\Phi\rangle$ [see Eq. (28)], the element $\rho^{(2)}_{\mathcal{KN}}$ is initially zero and remains zero for every $t$ [51]. As a result, from Eq. (31), $C_1$ remains negative at all times, in which case the concurrence for the initial state $|\Phi\rangle$ is given by $C_\Phi = C_2$. For $0 \leqslant a \leqslant 1$, one can easily prove that $C_\Phi$ is written as

$$C_\Phi(t) = 2\max[0, a\sqrt{1-a^2}|c_1(t)|^2]. \tag{32}$$

Following the same procedure for initial state $|\Psi\rangle$, we find that the density-matrix element $\rho^{(2)}_{\mathcal{LM}}$ is zero for all times $t$, in which case $C_2$ is always negative, giving $C_\Psi = C_1$. Thus, repeating the procedure for the calculation of the concurrence, we take

$$C_\Psi(t) = 2\max[0, \sqrt{1-a^2}|c_1(t)|^2 \times \{a - \sqrt{1-a^2}[1-|c_1(t)|^2]\}]. \tag{33}$$

### B. Numerical results for entanglement dynamics

In this section we present results for the dynamics of concurrence for the initial states of Eqs. (28) and (29). We begin, in Figs. 5 and 6, with the case of QDs with $\hbar\omega_1 = 4.16$ eV as qubits and initial state $|\Phi\rangle$ (Fig. 5) or $|\Psi\rangle$ (Fig. 6). In this and the figures that follow, we have used the results of $c_1(t)$ without implementing the RWA. In both cases we observe that for $t = 0$ and $a = 1/\sqrt{2}$ (dashed yellow curve) we have the maximum entanglement, which is expected since for that value of the parameter $a$ the initial states $|\Phi\rangle$ and $|\Psi\rangle$ become Bell states. Although this behavior is conserved for all times for the initial state $|\Phi\rangle$, this is not true for the other initial state, $|\Psi\rangle$; after some time, concurrence becomes more robust for $a = 0.9$ when compared with the case of $a = 1/\sqrt{2}$. In addition, concurrence for initial state $|\Phi\rangle$ seems to decay at approximately the same time for a certain distance, independent of the value of the parameter $a$. However, for the initial state $|\Psi\rangle$, the disentanglement time varies with the parameter $a$. More specifically, there is a finite disentanglement

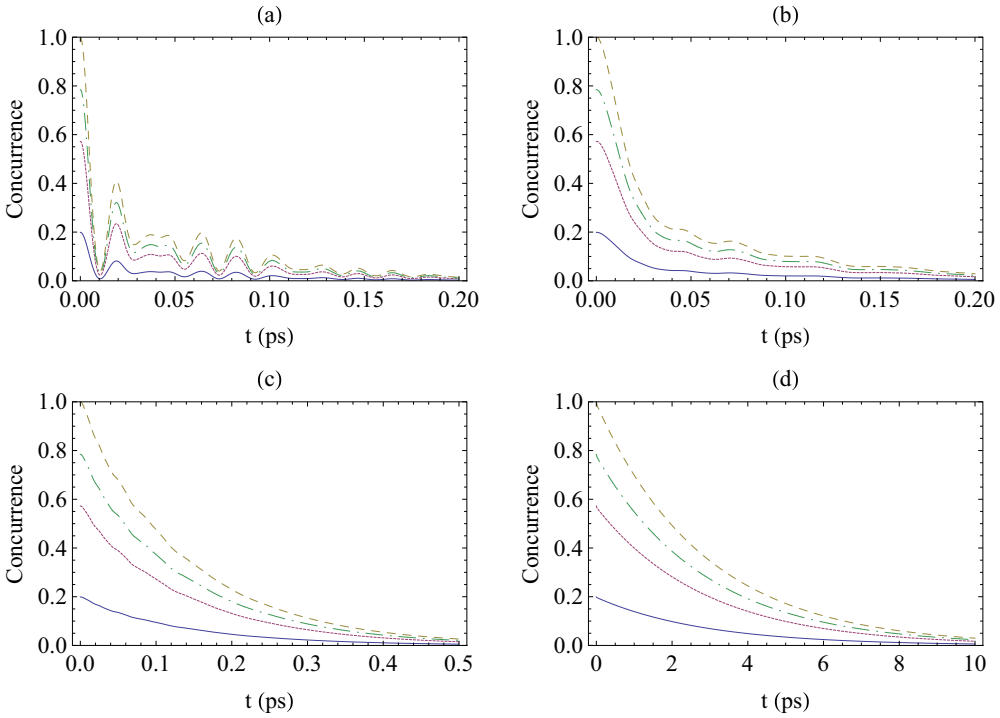


FIG. 5. (a) Time evolution of concurrence in the presence of the MNP for the initial state $|\Phi\rangle$ [Eq. (28)]. The qubits are QDs with $\hbar\omega_1 = 4.16\,\text{eV}$ and free-space decay time $\tau_0 = 4$ ns. The distance $D$ of each qubit from the MNP is (a) $D = 1$ nm, (b) $D = 2$ nm, (c) $D = 3$ nm, and (d) $D = 4$ nm. The four different curves correspond to four different values of the parameter $a$: solid blue curve for $a = 0.1$, dotted red curve for $a = 0.3$, dashed yellow curve for $a = 1/\sqrt{2}$, and dot-dashed green curve for $a = 0.9$.

time for $a = 0.1$ and $a = 0.3$, but there is no such time for $a = 1/\sqrt{2}$ and $a = 0.9$ for all distances of the qubits from the MNPs. This phenomenon is called entanglement sudden death (ESD), and it has been reported in many cases (see, for example, Refs. [48,54]).

We now turn our attention to the case in which our qubits are J-AGRs, again with $\hbar\omega_1 = 4.16\,\text{eV}$. We calculate the time evolution of concurrence for the same initial states as above; Fig. 7 shows the concurrence for the initial state $|\Phi\rangle$, and Fig. 8 shows that for the initial state $|\Psi\rangle$. For small distances

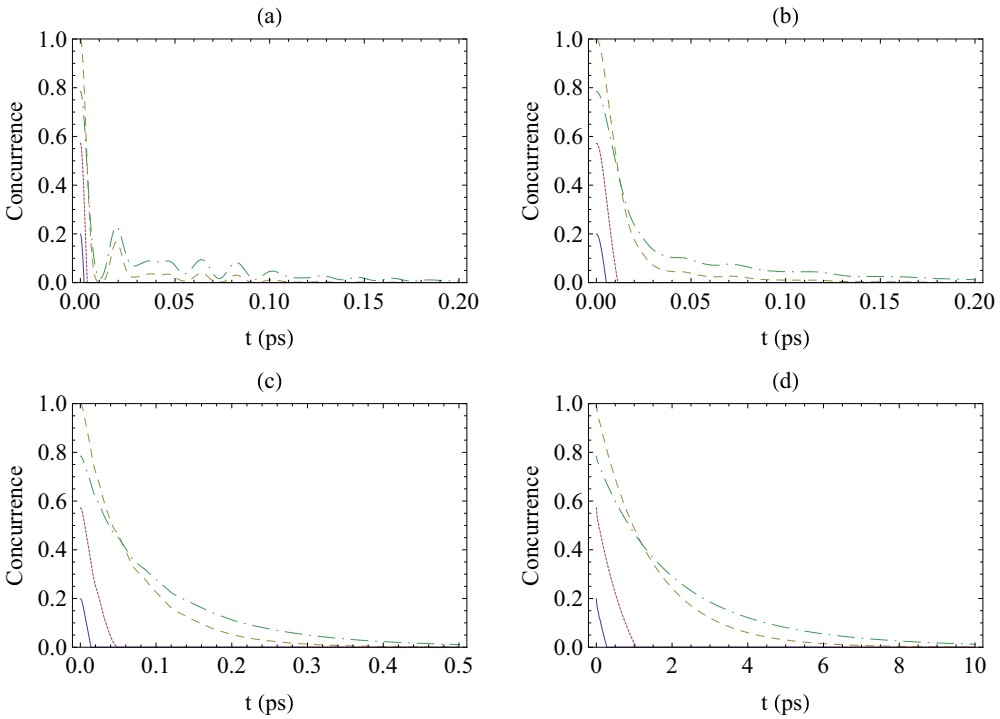


FIG. 6. The same as Fig. 5, but for the initial state $|\Psi\rangle$ of Eq. (29).

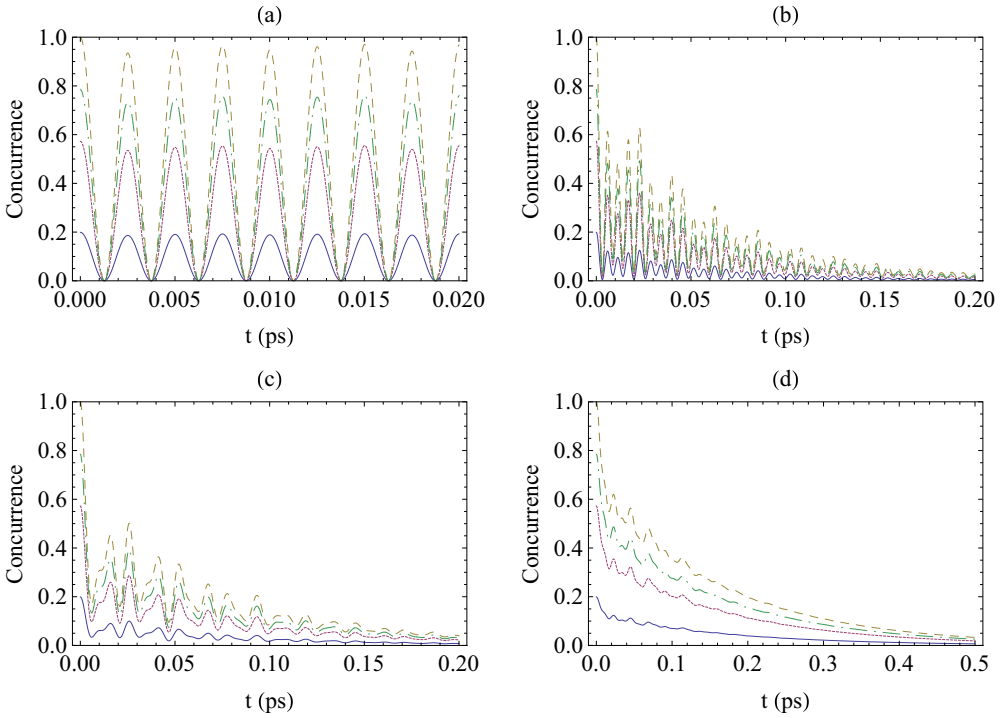


FIG. 7. The same as in Fig. 5, but for J-AGRs as qubits with $\hbar\omega_1 = 4.16\,\text{eV}$ and free-space decay time $\tau_0 = 70$ ps.

($D = 1$ nm) the concurrence has distinct zeros during its evolution for the initial state $|\Phi\rangle$ [see Fig. 7(a)]; however, it has certain periods of time that it is zero if the initial state is $|\Psi\rangle$ [see Fig. 8(a)]. We must stress here that the periods when concurrence becomes zero appear only for the values $a = 0.1$ and $a = 0.3$; otherwise, we have again distinct times when entanglement vanishes. Essentially, in Fig. 8(a) we observe again the phenomenon of ESD as in the case of QDs, but in addition, we see the revival of entanglement (or entanglement sudden birth) in a periodic way [49,66,67]. However, this does not occur if we move each qubit away from the corresponding MNP (e.g., at distances $D = 2$ nm, $D = 3$ nm, and $D = 5$ nm). ESD and revival of entanglement are not observed for the initial state $|\Phi\rangle$. For the initial state $|\Psi\rangle$, Figs. 8(b), 8(c) and 8(d)

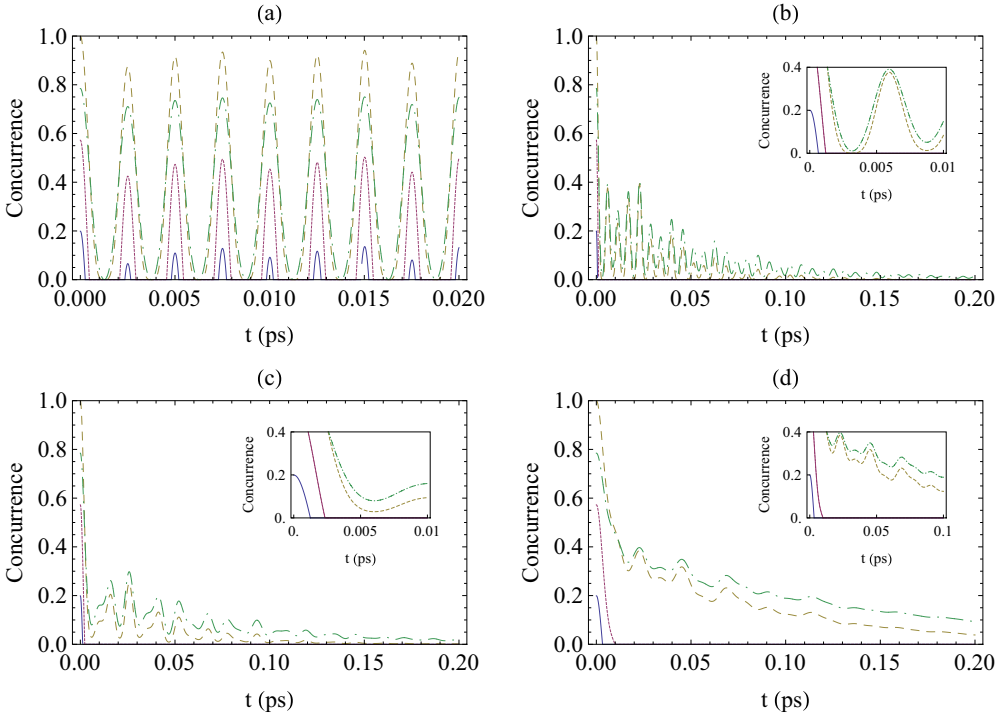


FIG. 8. The same as Fig. 7, but for the initial state $|\Psi\rangle$ of Eq. (29).

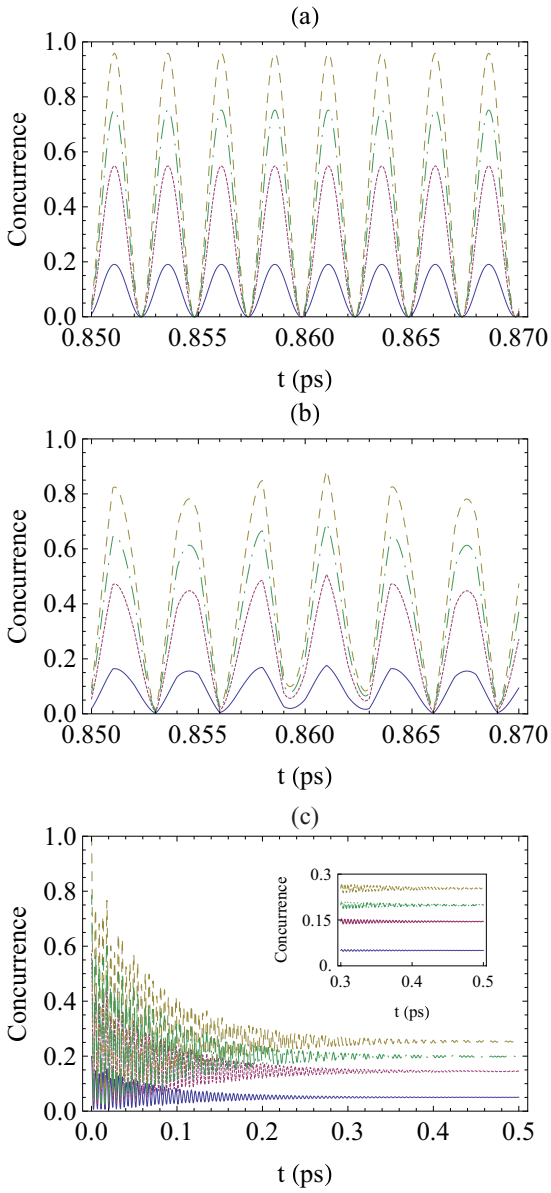


FIG. 9. (a) The same as in Fig. 7(a), but for the time interval $0.85 \leqslant t \leqslant 0.87$ ps. (b) The same as (a) but for distance $D = 1.5$ nm. (c) The same as 7(a) but for distance $D = 1.85$ nm.

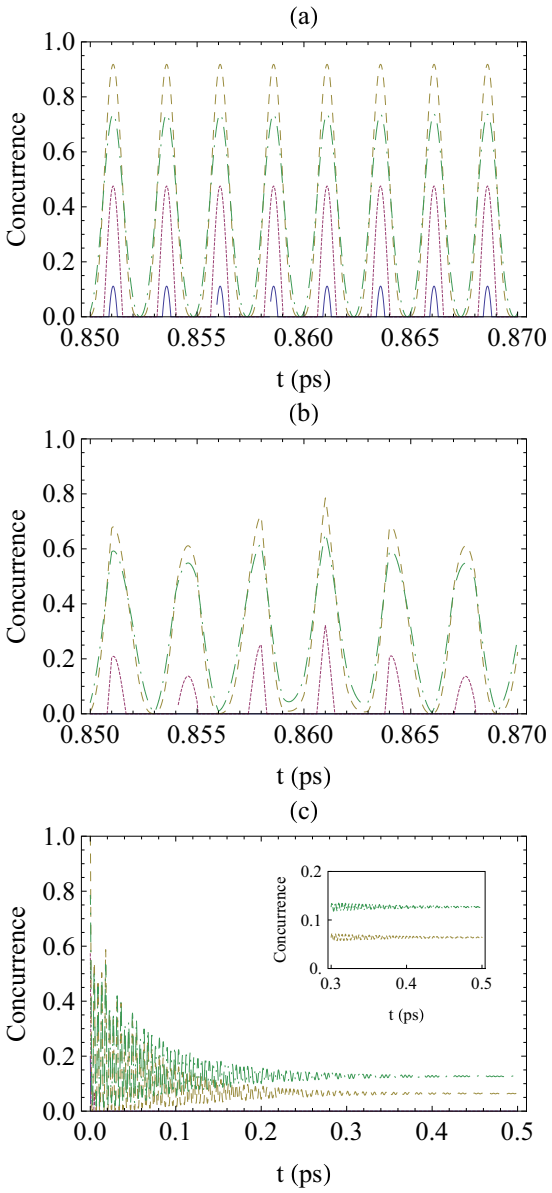


FIG. 10. The same as in Fig. 9, but for the initial state $|\Psi\rangle$.

display the phenomenon of ESD, which emerges only for $a = 0.1$ and $a = 0.3$ without the occurrence of a revival of entanglement for these distances. Besides ESD and revival of entanglement, another interesting effect here is the existence of entanglement oscillations [49,66,67] shown in Fig. 7(a). At larger distances, the non-Markovian character of the dynamics is still evident but somewhat weaker.

In Figs. 9 and 10 we further explore the concurrence dynamics for distances smaller than 2 nm. For the initial state $|\Phi\rangle$ entanglement oscillations are observed for all values of $a$ for larger time periods. However, for the initial state $|\Psi\rangle$ and for $D = 1$ nm, ESD is accompanied by a periodic entanglement revival [52] when $a = 0.1$ and $a = 0.3$. For the initial state $|\Psi\rangle$ for $a = 1/\sqrt{2}$ and $a = 0.9$, entanglement oscillations are observed. For $D = 1.5$ nm, a similar behavior with $D = 1$ nm is observed; however, the maximum values of concurrence are smaller. For $D = 1.85$ nm, the phenomenon of entanglement trapping is observed [51,53,55] since the oscillatory character of entanglement is lost in the long-time limit and the concurrence reaches a steady state.

As we observed above, four different phenomena occur here: ESD, periodic revival of entanglement, entanglement oscillations, and entanglement trapping, depending on the distance of the QE from the MNP and the initial state of the two-qubit system. It is interesting to examine whether there are any particular conditions for the emergence of these phenomena. When ESD is present, this means that concurrence takes a zero value at a specific time instant. From Eq. (32) we see that for any value of the parameter $a$, apart from the boundary values $a = 0$ and 1, the concurrence follows the time evolution of the population of the excited state, $|1\rangle$, multiplied by a constant which depends on $a$. As a result, whenever we

have population oscillations (or population trapping) in the long-time limit, we also have corresponding oscillations (or trapping) for the concurrence.

If the initial state is $|\Psi\rangle$ [see Eq. (29)], then entanglement is given by Eq. (33). Then, the necessary condition for zero entanglement at time $\tau$ is

$$|c_1(\tau)|^2 \leqslant 1 - \frac{a}{\sqrt{1-a^2}}. \tag{34}$$

Now we are interested in examining for which values of the parameter $a$ entanglement oscillations are preserved. We take, for example, the distance of each qubit from the MNP to be $D = 1.5$ nm. From Fig. 4(b) we see that the maximum value of the population $|c_1(t)|^2$, without implementing the RWA, is around 0.87. This means that, in order to have entanglement oscillations in the long-time limit, it should be $C_\Psi(t) > 0$. Thus, substituting the above value of the population, we find that, for this particular example, $a \geqslant 0.13$ in order to have nonzero concurrence. So we will observe three different regions in the time evolution of concurrence in this case. A characteristic small time interval of the time evolution is given in Fig. 10(b): for $a \leqslant 0.13$ we have no periodic entanglement revival in this longer time period, and as a result, only ESD takes place. For $0.13 \leqslant a \leqslant 1/\sqrt{2}$, both ESD and periodic entanglement revival occur, while for $a > 1/\sqrt{2}$ only entanglement oscillations are present. The boundary between the second and third regions was found by inserting the value $a = 1/\sqrt{2}$ in Eq. (34). For this value of the parameter $a$, the right-hand side of the inequality becomes zero, and $|c_1(t)|^2 < 0$, which cannot be true. Thus, for $a \geqslant 1/\sqrt{2}$ we have only entanglement oscillations. Of course, using a similar analysis, we can also find the corresponding regions when the quantum emitters are at distance $D = 1$ nm from the MNPs [Fig. 10(a)] and for any other value of the distance as well.

A similar analysis can be applied when we have entanglement trapping for the initial state $|\Psi\rangle$. Since trapping means that the concurrence has a steady state value at long times, using Eq. (33), we find that the condition for trapping at long times $T$ requires that $c_1(T)$ assumes a constant value; more specifically,

$$|c_1(T)|^2 > 1 - \frac{a}{\sqrt{1-a^2}}. \tag{35}$$

By inspecting Fig. 4(c) we observe that, without using the RWA approximation (red dashed curve), the population trapping is around $|c_1(T)|^2 \approx 0.2532$ at longer times. Thus, inserting this value in the above relation, we find that, for this particular example, the phenomenon of trapping takes place for $a \geqslant 0.598$. Therefore, entanglement trapping is obtained only for $a = 1/\sqrt{2}$ and $a = 0.9$, while for $a = 0.1$ only ESD occurs since Eq. (34) is satisfied. For $a = 0.3$, we observe the emergence of ESD at early times, as well as weak entanglement revivals at the oscillatory region of population dynamics; however, as time elapses, both phenomena disappear.

## IV. SUMMARY

We have studied the dynamics of a two-level quantum emitter next to a plasmonic nanoparticle. Namely, we have calculated the dynamics of the emitter without applying the Markovian and rotating-wave approximations by combining quantum dynamics calculations and classical electromagnetic calculations. We have shown that a transition from the non-Markovian regime to the Markovian regime takes place when varying the distance between the quantum emitter and the MNP. At the same time, we have studied the role of the RWA for two different types of quantum emitters, QDs and J-AGRs. For QDs, non-Markovian effects are observed for small interparticle distances, in which case the RWA is adequate, while for J-AGRs much stronger non-Markovian dynamics is observed; at the same time, the RWA fails for very small distances between the quantum emitter and the MNP, while for larger distances (typically, above 3 nm) it is still a valid approximation.

We have also studied the entanglement dynamics of two initially entangled qubits interacting independently with a MNP. Using the two-level quantum dynamics results without the RWA, we have shown that the entanglement dynamics may have a strong non-Markovian response. Several phenomena are identified for different initial two-qubit states and different distances between the qubits and the MNP, such as ESD, periodic entanglement revival, entanglement oscillations, and entanglement trapping. We believe that the present work will be useful in the area of quantum technology.

## ACKNOWLEDGMENTS

N.I. acknowledges the support of his Ph.D. by the General Secretariat for Research and Technology (GSRT) and the Hellenic Foundation for Research and Innovation (HFRI) via a doctoral scholarship (Grant No. 2649).

[1] M. S. Tame, K. R. McEnery, S. K. Ozdemir, J. Lee, S. A. Maier, and M. S. Kim, Nat. Phys. **9**, 329 (2013).
[2] P. Törmä and W. L. Barnes, Rep. Prog. Phys. **78**, 013901 (2015).
[3] F. Marquier, C. Sauvan, and J.-J. Greffet, ACS Photonics **4**, 2091 (2017).
[4] P. Vasa and C. Lienau, ACS Photonics **5**, 2 (2018).
[5] A. Gonzalez-Tudela, F. J. Rodriguez, L. Quiroga, and C. Tejedor, Phys. Rev. B **82**, 115334 (2010).
[6] A. González-Tudela, P. A. Huidobro, L. Martín-Moreno, C. Tejedor, and F. J. García-Vidal, Phys. Rev. B **89**, 041402(R) (2014).
[7] J. Hakami, L. Wang, and M. S. Zubairy, Phys. Rev. A **89**, 053835 (2014).
[8] R.-C. Ge and S. Hughes, Phys. Rev. B **92**, 205420 (2015).
[9] J. Hakami and M. S. Zubairy, Phys. Rev. A **93**, 022320 (2016).
[10] H. Varguet, B. Rousseaux, D. Dzsotjan, H. R. Jauslin, S. Guérin, and G. C. des Francs, Opt. Lett. **41**, 4480 (2016).
[11] R.-Q. Li, D. Hernangomez-Perez, F. J. Garcia-Vidal, and A. I. Fernandez-Dominguez, Phys. Rev. Lett. **117**, 107401 (2016).
[12] I. Thanopulos, V. Yannopapas, and E. Paspalakis, Phys. Rev. B **95**, 075412 (2017).

[13] I. Liberal and N. Engheta, Proc. Natl. Acad. Sci. USA **114**, 822 (2017).
[14] C.-J. Yang and J.-H. An, Phys. Rev. B **95**, 161408(R) (2017).
[15] R.-Q. Li, F. J. Garcia-Vidal, and A. I. Fernandez-Dominguez, ACS Photonics **5**, 177 (2018).
[16] M. Hensen, T. Heilpern, S. K. Gray, and W. Pfeffer, ACS Photonics **5**, 240 (2018).
[17] R. Chikkaraddy, B. Nijs, F. Benz, S. J. Barrow, O. A. Scherman, E. Rosta, A. Demetriadou, P. Fox, O. Hess, and J. J. Baumberg, Nature (London) **535**, 127 (2016).
[18] K. Santhosh, O. Bitton, L. Chuntonov, and G. Haran, Nat. Commun. **7**, 11823 (2016).
[19] R. Liu, Z.-K. Zhou, Y.-C. Yu, T. Zhang, H. Wang, G. Liu, Y. Wei, H. Chen, and X.-H. Wang, Phys. Rev. Lett. **118**, 237401 (2017).
[20] S. I. Bozhevolnyi and J. B. Khurgin, Nat. Photonics **11**, 398 (2017).
[21] C. Racknor, M. R. Singh, Y. Zhang, D. J. S. Birch, and Y. Chen, Methods Appl. Fluoresc. **2**, 015002 (2014).
[22] M. R. Singh, J. Guo, J. M. J. Cid, and J. E. De H. Martinez, J. Appl. Phys. **121**, 094303 (2017).
[23] M. R. Singh, M. C. Sekhar, S. Balakrishnan, and S. Masood, J. Appl. Phys. **122**, 034306 (2017).
[24] A. Gonzalez-Tudela, D. Martin-Cano, E. Moreno, L. Martin-Moreno, C. Tejedor, and F. J. Garcia-Vidal, Phys. Rev. Lett. **106**, 020501 (2011).
[25] D. Martin-Cano, A. Gonzalez-Tudela, L. Martin-Moreno, F. J. Garcia-Vidal, C. Tejedor, and E. Moreno, Phys. Rev. B **84**, 235306 (2011).
[26] J. Xu, M. Al-Amri, Y. Yang, S.-Y. Zhu, and M. S. Zubairy, Phys. Rev. A **84**, 032334 (2011).
[27] Y. He and K.-D. Zhu, Nanoscale Res. Lett. **7**, 95 (2012).
[28] A. Gonzalez-Tudela, D. Martin-Cano, E. Moreno, L. Martin-Moreno, F. J. Garcia-Vidal, and C. Tejedor, Phys. Status Solidi C **9**, 1303 (2012).
[29] C. E. Susa, J. H. Reina, and L. L. Sanchez-Soto, J. Phys. B **46**, 224022 (2013).
[30] Q.-L. He, J.-B. Xu, and D.-X. Yao, Quantum Inf. Process. **12**, 3023 (2013).
[31] S.-P. Liu, J.-H. Li, R. Yu, and Y. Wu, Phys. Rev. A **87**, 042306 (2013).
[32] C. Lee, M. Tame, C. Noh, J. Lim, S. A. Maier, J. Lee, and D. G. Angelakis, New J. Phys. **15**, 083017 (2013).
[33] C. E. Susa, J. H. Reina, and R. Hildner, Phys. Lett. A **378**, 2371 (2014).
[34] J. Hou, K. Slowik, F. Lederer, and C. Rockstuhl, Phys. Rev. B **89**, 235413 (2014).
[35] K. V. Nerkararyan and S. I. Bozhevolnyi, Phys. Rev. B **92**, 045410 (2015).
[36] S. A. H. Gangaraj, A. Nemilentsau, G. W. Hanson, and S. Hughes, Opt. Express **23**, 22330 (2015).
[37] W.-L. Yang, J.-H. An, C.-J. Zhang, C.-Y. Chen, and C. H. Oh, Sci. Rep. **5**, 15513 (2015).
[38] M. Otten, R. A. Shah, N. F. Scherer, M. Min, M. Pelton, and S. K. Gray, Phys. Rev. B **92**, 125432 (2015).
[39] X. Zeng, Z. Liao, M. Al-Amri, and M. S. Zubairy, Europhys. Lett. **115**, 14002 (2016).
[40] N. Iliopoulos, A. F. Terzis, V. Yannopapas, and E. Paspalakis, Ann. Phys. (NY) **365**, 38 (2016).
[41] Z.-D. Hu, X. Liang, J. Wang, and Y. Zhang, Opt. Express **24**, 10817 (2016).
[42] M. Otten, J. Larson, M. Min, S. M. Wild, M. Pelton, and S. K. Gray, Phys. Rev. A **94**, 022312 (2016).
[43] F. Zhang, D. X. Zhao, Y. Gu, H. Chen, X. Hu, and Q. H. Gong, J. Appl. Phys. **121**, 203105 (2017).
[44] N. Iliopoulos, A. F. Terzis, V. Yannopapas, and E. Paspalakis, Phys. Rev. B **96**, 075405 (2017).
[45] H. Zheng, S. Y. Zhu, and M. S. Zubairy, Phys. Rev. Lett. **101**, 200404 (2008).
[46] Z.-H. Li, D.-W. Wang, H. Zheng, S.-Y. Zhu, and M. S. Zubairy, Phys. Rev. A **80**, 023801 (2009).
[47] S. Yang, M. Al-Amri, S.-Y. Zhu, and M. S. Zubairy, Phys. Rev. A **87**, 033818 (2013).
[48] T. Yu and J. H. Eberly, Phys. Rev. Lett. **93**, 140404 (2004).
[49] M. Yönac, T. Yu, and J. H. Eberly, J. Phys. B **39**, S621 (2006).
[50] B. Bellomo, R. Lo Franco, and G. Compagno, Phys. Rev. Lett. **99**, 160502 (2007).
[51] B. Bellomo, R. Lo Franco, S. Maniscalco, and G. Compagno, Phys. Rev. A **78**, 060302 (2008).
[52] B. Bellomo, R. Lo Franco, and G. Compagno, Phys. Rev. A **77**, 032342 (2008).
[53] B. Bellomo, R. Lo Franco, S. Maniscalco, and G. Compagno, Phys. Scr. A **2010**, 014014 (2010).
[54] T. Yu and J. H. Eberly, Science **323**, 598 (2009).
[55] Q.-J. Tong, J.-H. An, H.-G. Luo, and C.-H. Oh, Phys. Rev. A **81**, 052330 (2010).
[56] R. Lo Franco, B. Bellomo, S. Maniscalco, and G. Compagno, Int. J. Mod. Phys. B **27**, 1345053 (2013).
[57] W. K. Wootters, Phys. Rev. Lett. **80**, 2245 (1998).
[58] S. Scheel and S. Y. Buhmann, Acta Phys. Slovaca **58**, 675 (2008).
[59] H. T. Dung, L. Knöll, and D.-G. Welsch, Phys. Rev. A **62**, 053804 (2000).
[60] H. T. Dung, L. Knöll, and D.-G. Welsch, Phys. Rev. A **57**, 3931 (1998).
[61] E. Almpanis and N. Papanikolaou, J. Appl. Phys. **114**, 083106 (2013).
[62] V. Yannopapas and N. V. Vitanov, Phys. Rev. B **75**, 115124 (2007).
[63] A. V. Akimov, A. Mukherjee, C. L. Yu, D. E. Chang, A. S. Zibrov, P. R. Jemmer, H. Park, and M. D. Lukin, Nature (London) **450**, 402 (2007).
[64] H. Fidder, J. Knoester, and D. A. Wiersma, Chem. Phys. Lett. **171**, 529 (1990).
[65] I. Thanopulos, P. Brumer, and M. Shapiro, J. Phys. Chem. **133**, 154111 (2010); X. Li, I. Thanopulos, and M. Shapiro, Phys. Rev. A **83**, 033415 (2011).
[66] Z.-X. Man, Y.-J. Xia, and N. B. An, J. Phys. B **41**, 085503 (2008).
[67] Q.-H. Chen, Y. Yang, T. Liu, and K.-L. Wang, Phys. Rev. A **82**, 052306 (2010).